Proceedings of GPPS Forum 18
Global Power and Propulsion Society
Montreal, 7th-9th May 2018
www.gpps.global

GPPS-2018-0040

EFFECTS OF STATOR PLATFORM GEOMETRY FEATURES ON BLADE ROW PERFORMANCE

Derek J Taylor
Whittle laboratory
University of Cambridge
taylor.derekjames@gmail.com
Cambridge CB3 0DY, England

John P Longley
Whittle laboratory
University of Cambridge
jpl@eng.cam.ac.uk
Cambridge CB3 0DY, England

ABSTRACT

Real geometry features such as shroud cavities, inter-platform and vane-pack gaps can affect the hub endwall flow through compressor blade rows. Additionally, misalignment of the platform endwalls due to manufacturing tolerances can be important. This paper details an experimental and computational investigation of these effects. To ensure that the measurements were representative a novel experimental technique was developed to generate end-wall skew in the linear cascade. Without the presence of the endwall boundary layer skew the cascade flow did not capture the flow features typically observed in multi-stage compressor operation.

The skew generation method involves injecting flow along the endwall in such a manner as to control both the displacement thickness and tangential momentum thickness of the resulting boundary layer. The study reveals that real geometry features can have a significant impact on the flowfield within a blade passage. For stator shrouds, increasing leakage flow rates increases the stagnation pressure loss coefficient however, increasing the level of whirl pickup of the leakage flow can offset the natural secondary flow and thus reduce the loss. All of the steps and gaps that were found to be present in real compressors were found to increase the losses relative to a smooth endwall. It is also shown that CFD simulations are capable in capturing the trends observed in the experiments.

INTRODUCTION

The International Air Transport Association [IATA, 2017] forecast that in 2018 fuel bills for airlines will account for 19.6% of average operating costs, totalling $156 billion. Between this expenditure and the drive to reduce greenhouse gas emissions, there is a large incentive to reduce fuel burn. There are a number of avenues being explored to reduce this cost, including reduced airframe drag and optimised flight plans. Improvements in aero-engine efficiency will also lead to reduced fuel burn through more efficient combustion and improved component efficiencies. This paper focuses on geometry features within axial compressors that have an effect on the blade row performance and efficiency.

The construction and assembly of an axial compressor blade row introduces a number of features that are likely undesirable from an aerodynamic standpoint. A complex leakage path exists beneath the stator shroud. While the effect of shroud leakage is usually considered in the design, it is not always fully modelled and therefore the complexities of the leakage flow rate and the whirl pick-up may not always be captured.

Stator blades are typically manufactured individually, with an integral hub platform. Groups of 5-8 blades are then assembled into vane-packs by welding them together at the casing. The hub platforms are not welded together to allow for the effects of vibration and thermal expansion. This results in an axial inter-platform gap at the hub between each blade row, which is estimated to up to 1% of pitch. These gaps are usually not included in the design and their effects are unknown. Due to manufacturing tolerances, hub endwalls can experience misalignments along the inter-platform gaps resulting in a step in the flow path. These steps have been estimated to be in the order of 1% of span.

The vane-packs are then slotted into a ring, but gaps are also left between the packs to allow for vibration and expansion. These vane-pack gaps are estimated to be of the order of 10% of pitch. Finally the hub platforms are located in a circular c-ring, which is usually manufactured in two parts, also resulting in a leakage flow path.

This paper will firstly focus of the impact of the shroud leakage flow and the associated whirl pick-up. Secondly, the impact of the inter-platform gaps, vane-pack gaps and misaligned endwalls will be investigated.

Literature Review

The sources of loss within turbomachines have been the subject of extensive study. Denton (1993) classified the losses within blade rows into three categories, profile, leakage and secondary losses, however the interaction of

leakage and endwall flows can make the latter two hard to separate. A review of secondary flows and the resulting losses was produced by Sieverding (1984) and Gbadebo et al. (2004) furthered the studies detailing the 3D nature of the flowfields. These papers show how boundary layer flow on the endwalls is overturned relative to the mainstream flow by the blade pressure field. These secondary flows interact with the blade suction surface forming loss cores in the corners between the blade and endwalls.

There have been a number of studies into shroud leakage flows, including LeJambre et al. (1995), Heidegger et al. (1996) and Wellborn and Okiishi (1998). Demargne and Longley (2000) investigated the impact shroud leakage flows, but included the effect of the tangential momentum of leakage flows on blade row losses. All these studies showed that low axial momentum flow impinging the hub endwall increases the secondary flow, increasing the interaction of the endwall flows with the suction surface of the blade leading to larger loss cores and lower efficiencies. However, the tangential momentum of the leakage flow (due to whirl pickup on the shroud cavity) can help to resist the cross passage movement of the secondary flows in a compressor.

Studies into the impact of endwall geometry features such as gaps and steps have predominately been done on turbine geometries. Reid et al. (2005) investigated the impact of inter-platform gaps and found that they could reduce stage efficiency by 0.5-1.5%. Grewe et al. (2014) showed how steps along an inter-platform gap, regardless of their orientation, will increase the losses in a blade row.

Other than profiled endwalls, to the author's knowledge the impact of gaps and steps within compressors have not been studied. Considering larger scale geometry features, Johnson and Greitzer (1987) showed that the adverse pressure gradient in a compressor caused flow within slotted hub and casing treatments to be ingested near the trailing edge and reinjected near the leading edge. Leishman et al. (2004) studied the impact of bleed off-takes locate within a blade passage and described how, even with no net bleed, flow moved in and out of the bleed slots.

METHODOLOGY

The real-geometry features described above are investigated through a combination of experimental testing on a linear cascade and computational investigations.

Experimental Setup

The linear cascade uses prismatic blades, with a 2D profile coming from a section of a 3D blade developed for a low-speed investigation of an aero-engine geometry. The section chosen was from 15% of span above the hub as this gives a representative pressure field on the hub platforms. Details of the blading are given in Table 1. The aerofoils are wire cut aluminium and slotted into 3D printed hub platforms. The centre two blades can be removed allowing different platform geometries to be tested. The cascade has a shroud leakage cavity with adjustable seal clearance. The shroud walls beneath the stators are not rotating so a method is needed to control the velocities within the shroud cavities to simulate whirl pick-up. A closed loop recirculation system with in-line fans to control the velocities was fitted. The leakage flow rate is determined by the pressure difference across the stator and the level of whirl pick-up is controlled by the recirculation system. It is expected that the whirl velocity in the downstream cavity will be equal to that of the mainstream flow being ingested, which for the compressor design is roughly 0.15U, where U is the notional hub wheel-speed. The whirl velocity in the upstream shroud cavity can be varied between 0.2U to 0.8U. A schematic of the cascade and the recirculation systems as well as a picture of the working section of the cascade are shown in Figure 1.

The cascade has a novel system for skewing the boundary layer of the mainstream flow upstream of the shroud cavities which is discussed in a later section.

Table 1: Cascade blade geometry

Span	225 mm
Chord	199.5 mm
Pitch to chord ratio	0.55
Blade inlet metal angle	56.9°
Inlet flow angle	45°
Blade exit metal angle	11.7°
Reynolds number (chord)	3.50×10^5

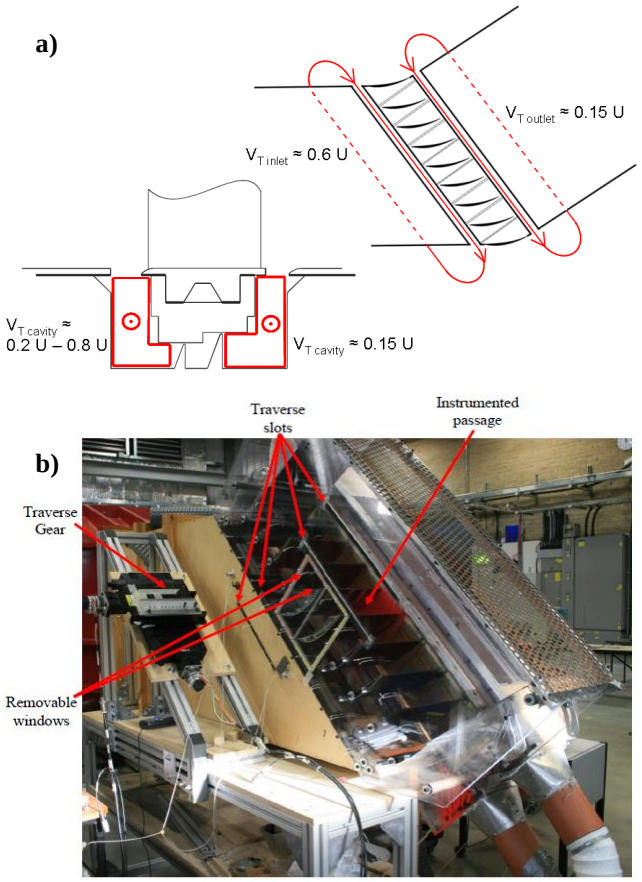

Figure 1: a) Schematic of cascade shroud assembly and control of cavity velocities and b) working section setup

The bulk of the cascade measurement data is in the form of traverses using a calibrated 5-hole probe. Tests of the measurement repeatability from the probe were made both in

the calibration wind tunnel and in the test rig. The results showed that the stagnation pressure coefficient could be measured repeatedly to within ±0.15% of dynamic head. Traverses were undertaken upstream of the shroud cavity to capture the inlet flowfield and downstream of the blade trailing edge to capture the resulting blade flowfield.

Computational Fluid Dynamics

The Rolls-Royce proprietary code, HYDRA [Lapworth, 2004], was used for all CFD simulations. This is a general purpose flow solver for hybrid unstructured meshes. The Spalart-Allmaras turbulence model, which was specifically designed for aerodynamic flows and which has been found to be successful for practical turbomachinery flows [Casey and Wintergeste, 2000] has been used for all simulations.

The calculation domains are shown in Figure 2. The inlet boundary matches the location of the upstream traverse plane on the cascade and the measured inlet profiles of total pressure, temperature and flow angles were used. A uniform static pressure, consistent with that measured in the cascade, was used for the exit boundary. Details of the boundaries for the shroud cavities are given below.

A mesh sensitivity study was performed on the geometry shown in Figure 2a. The solid surfaces are covered with a layer of prismatic cells to capture the boundary layer, while the rest of the volume is meshed with tetrahedral. The maximum y^+, occurring at peak velocity on the blade surface, was seven which ensured the boundary layer is resolved. The tetrahedral volume mesh was then refined until no further changes in the solution were seen. The final model contained roughly 14.2 million elements, comprising of 8.6 million prismatic cells and 5.5 million tetrahedral.

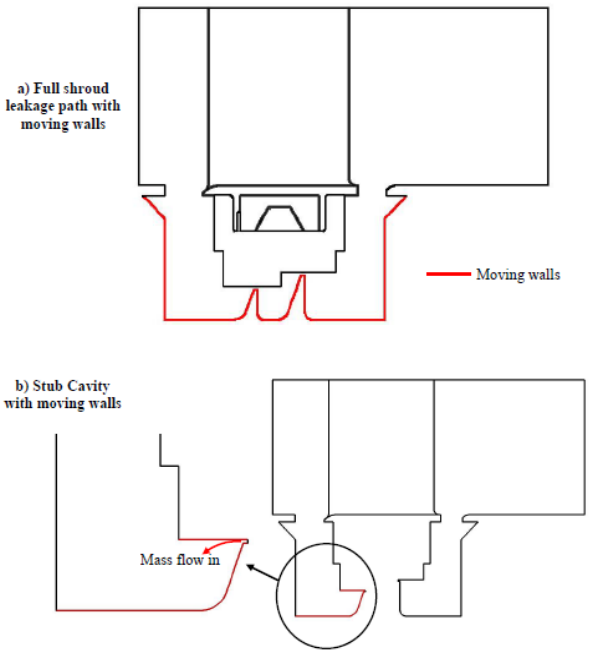

Figure 2: CFD geometry: a) full shroud cavity to determine leakage flow rates; b) stub cavities to fix leakage flow rate and set cavity tangential velocity.

Like the cascade, the complete solution domain has a full shroud cavity and the endwalls are stationary so a method of controlling the cavity tangential velocities is required. To achieve this, one complete domain is calculated at the required fin seal clearance with a moving wall in the cavity. This is used to determine the leakage flow rate through the fin seals. The geometry is then modified by removing the two fin seals. An extra outflow boundary is placed at the front edge of the rear seal and an extra inflow boundary is placed at the rear edge of the front seal. Through these boundaries the required mass flow is specified and at the inlet boundary the required tangential velocity is set. This method allows the required cavity conditions to be specified. The complete CFD domain and the method for simulating the cavity whirl pick-up are shown in Figure 2.

For the stub cavity calculations shown in Figure 2b, it was necessary to translate the walls shown in red at a speed equivalent to the tangential velocity specified at the mass flow inlet boundary. Without these moving walls it was found that the prescribed tangential velocity did not advance through the cavity. Likewise with zero fin seal clearance, the tangential velocity did not wash through the cavity and hence this case was not calculated.

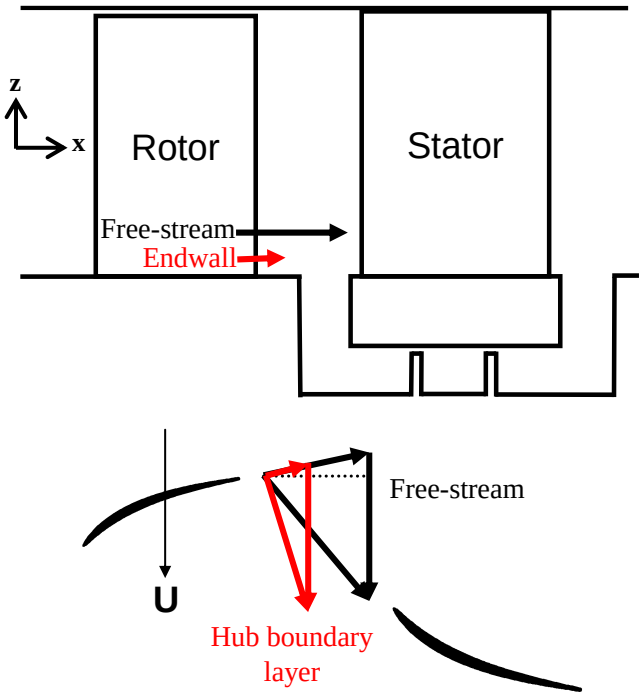

Figure 3: Boundary layer caused by change in frame of reference

Boundary Layer Skew

A standard linear cascade will produce a uni-directional flowfield such that the incidence onto the blade will be uniform along the span. However, it is known that in a compressor the endwall boundary layer flow is skewed relative to the mainstream. As demonstrated below, skew can have a profound effect on the secondary flows in the downstream blade row. To be relevant to aero-engines the cascade needs to include a skewed boundary layer.

Secondary flows can skew the hub endwall boundary layer relative to the mainstream, however it is also caused by the change in frame of reference between moving and stationary blades. The simplified example, Figure 3, shows the velocity triangles at rotor exit/stator inlet in the free-stream, just above the boundary layer, and in the boundary layer just above the hub. Assuming that the exit relative flow angle is uniform along the span, the axial and relative velocities reduce in the boundary layer, but the wheel speed is effectively unchanged resulting in a skewing of the absolute velocity vector. This also satisfies the non-slip condition on the rotor hub platform that the fluid on the wall will move in a tangential direction.

To understand the impact of not modelling this skewed boundary layer, consider the contour plots from CFD calculations shown in Figure 4. These show the flowfield (in terms of total pressure coefficient) for a) the design case from the 3 stage compressor with a skewed boundary layer, b) the above blade in a linear cascade with the same mainstream flow, but the skew removed from the boundary layer, i.e. what would be expected in a cascade and c) the above case but with shroud leakage flow (0.5% of mainstream flow) injected upstream of the blade row.

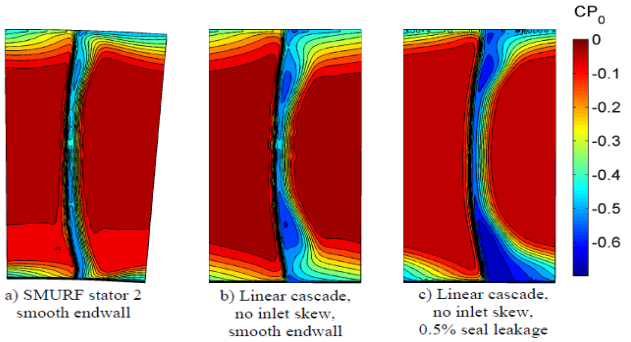

Figure 4: Contour plots of stagnation pressure coefficient at the trailing edge from CFD results showing effect of removing inlet boundary layer skew

Removing the boundary layer skew has resulted in significantly stronger secondary flows. The addition of low momentum leakage flow onto the hub further exacerbates the issue. The end result is a flowfield which is not representative of a real compressor and therefore any measurements would be of little practical use.

In order to understand the influence of boundary layer skew and to be able to recreate it in a cascade, it is necessary to quantify it. Mager (1951) presented a series of equations that define a boundary layer in a cross flow, however these were in a coordinate system aligned with the mainstream flow. Here the equations are defined in terms of the axial and tangential velocities. The boundary layer displacement thickness is defined using:

$$\delta^* = \int_0^{\Delta z} \left(1 - \frac{v_x}{V_x}\right) dz \qquad (1)$$

Similarly the axial momentum thickness can be defined:

$$\theta_x = \int_0^{\Delta z} \frac{v_x}{V_x}\left(1 - \frac{v_x}{V_x}\right) dz \qquad (2)$$

It is possible to quantify the tangential momentum using a similar equation. However, if the freestream tangential velocity is zero the equation is singular. Instead:

$$\theta_y = \int_0^{\Delta z} \frac{v_x}{V_x}\left(\frac{V_y - v_y}{V_x}\right) dz \qquad (3)$$

There have been a number of studies into the effects of boundary layer skew. Moore and Richardson (1957) were the first to publish a study and it was shown that the natural skewing of the boundary layer in a compressor acts to off-set the secondary flows by opposing the turning of the flow on the endwall. Walsh and Gregory-Smith (1990) also demonstrated that the loss in an axial compressor is dependent on the level of boundary layer skew.

A set of target inlet boundary conditions for the cascade were generated based on CFD calculations for the design operating point of a low-speed 3 stage axial compressor. The boundary layer displacement and momentum thicknesses, calculated using Eqns 1-3 are given in Table 2 for the tip (collateral) and hub (skewed) boundary layers. The skewed boundary layer has a negative tangential momentum thickness which corresponds to a tangential momentum greater than the mainstream.

Table 2: Comparison of boundary layer parameters for a collateral and a skewed boundary layer

	Hub	Casing
δ^*/Span	1.61 %	1.61 %
θ_x/Span	0.84 %	0.84 %
θ_y/Span	-0.86 %	0.84 %

Skew generation in the cascade

Different studies have used various methods to introduce boundary layer skewing in a cascade, from multiple cross-blowing jets [Moore and Richardson, 1957] to moving endwalls [Rushton, 2003], however a simpler method was desired for these experiments.

The method developed for these studies involves injecting flow through a 5% of span backwards facing step along the hub endwall at angle to the mainstream such that the injected axial and tangential velocities would give the desired boundary layer.

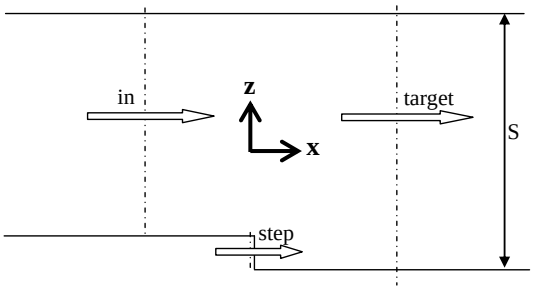

Figure 5: Control volume calculation of step injection requirements

The required axial and tangential velocities through the step can be calculated by considering the control volume shown in Figure 5. Using conservation of mass and a knowledge of the displacement thickness at inlet ('in') and the target conditions, it is possible to calculate $V_{x,step}$. Also, through conservation of tangential momentum, it is possible to calculate the required tangential velocity though the step in order to obtain the target tangential momentum thickness. This ensures that the flow injected from the step gives the correct axial displacement thickness and tangential momentum thickness. The axial momentum thickness cannot be controlled by this method and measurements in the cascade showed that it was slightly higher than the target conditions at 1.2% of span compared to 0.85%. While this resulted in slightly higher secondary losses than intended, the flowfield was still representative of the design intent.

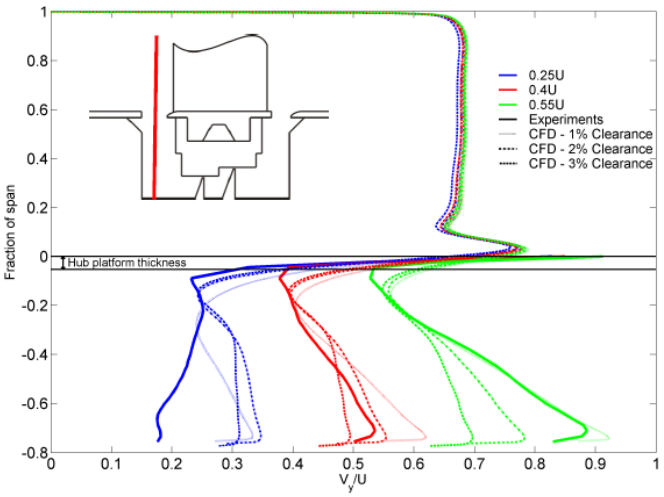

Figure 6: Comparison of spanwise profiles of upstream cavity tangential velocity between CFD and experiments

Shroud Cavity Effects

The experimental and computational investigation into the impact of shroud leakage and whirl pick-up took the form of a matrix of tests. Four seal clearances were intended for both test and CFD at 0%, 1%, 2% and 3% of span. However, a setup error resulted in the largest clearance tested in the cascade to be only 2.5% and for reasons stated in the methodology section it was not possible to obtain a converged result in CFD with 0% clearance. At each of the tested seal clearances, the tangential velocity in the upstream cavity (at 15% of span below the hub) was set to 0.25U, 0.4U and 0.55U. The spanwise profile of tangential velocity from the casing down into the shroud cavity, for the CFD and experiments, is shown in Figure 6.

There is a good match at all upstream cavity velocities, particularly in the region just beneath the hub. As it is this flow that will be injected into the mainstream, Figure 6 gives confidence that the CFD is matching the experiments well. It should be noted however, that the tests show a higher tangential velocity at the hub line than the CFD calculates. The CFD predicts greater mixing of the boundary layer and cavity flows reducing the peak tangential velocity at blade inlet, whereas the experiments show less mixing and higher tangential velocities at the leading edge. This will have an impact on the result with the CFD being less able to resist the turning of the secondary flow.

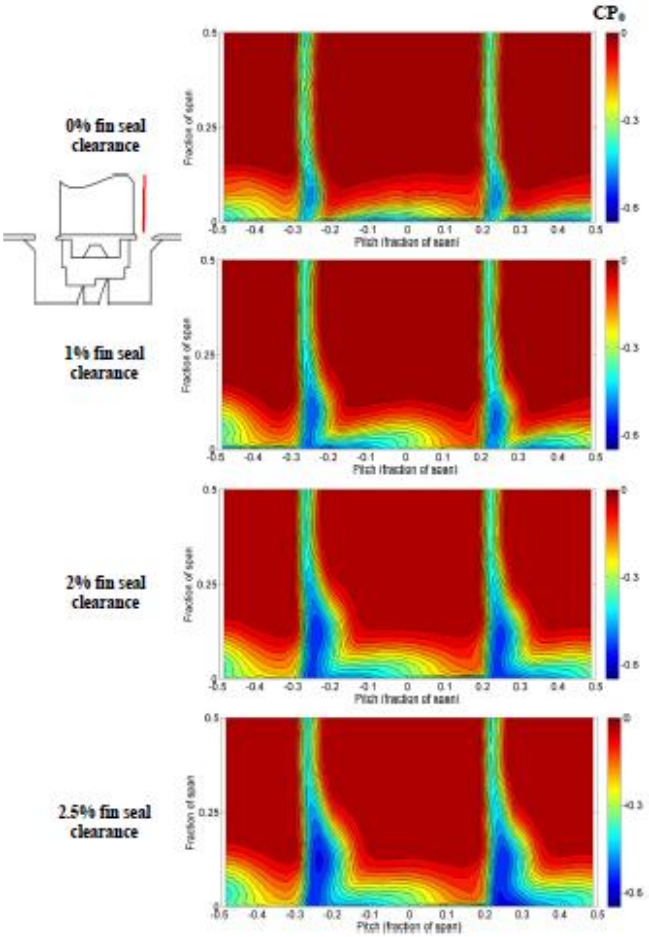

Figure 7: Effect on stagnation pressure coefficient of changing fin seal clearance

Effect of seal clearance

Consider the case with just the seal clearance varying and the upstream cavity tangential velocity fixed at 0.4U. Figure 7 shows contour plots of stagnation pressure coefficient measured just downstream of the blade trailing edge at three different fin seal clearances. The first point to note is that the 0% and 1% fin seal clearances cases show a good resemblance to the design flowfield shown previously in Figure 4, indicating that the presence of the generate skewed boundary layer is working as designed.

It is clear from Figure 7 that as the fin seal clearance increased, the strength of the secondary flows also increased resulting in larger loss cores at the trailing edge. This is due to the increasing volume of low momentum flow being introduced onto the stator hub which is then being swept across the blade passage onto the suction surface.

The CFD results (not shown) give a similar result, although the calculations show lower stagnation pressure within the loss cores and along the hub walls. This is due to the CFD calculation being fully turbulent which results in higher boundary layer losses.

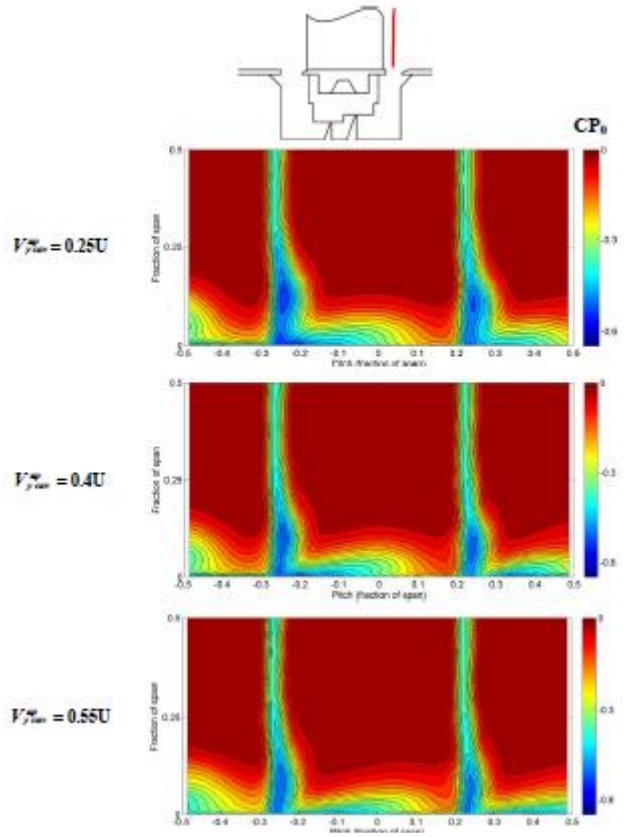

Figure 8: Effect on stagnation pressure coefficient of changing fixed upstream cavity tangential velocity

Effect of upstream cavity tangential velocity

Figure 8 shows the measured impact of changing the upstream cavity tangential velocity for a fixed fin seal clearance (1%). The results show that as the upstream cavity tangential velocity increases the strength and size of the loss core at the hub corners is reduced indicating that the increased momentum of the injected leakage flow is more able to resist the cross-passage pressure gradient.

Demargne and Longley (2000) saw a similar effect of reduced losses with increasing upstream cavity tangential velocity, although their results did not show any levelling off of the improvement. However the experiments reported in that paper were done in the absence of a realistically skewed inlet boundary layer, and therefore did not have the increased tangential momentum in the boundary layer as presented above. It is possible that if the Demargne and Longley experiments had been run to even higher upstream cavity tangential velocities then they may too have seen a levelling off of the results.

The largest change is seen between the cases with 0.25U and 0.4U. The CFD shows similar changes in the flowfield with increasing cavity velocities, but it also doesn't show the levelling off of the improvements seen in the experiments. This is most likely due to the increased mixing of the hub flow upstream of the leading edge which reduced the peak tangential velocity in the CFD relative to the experiments.

Overall impact of shroud cavity flows

The results presented above show the trends in the flowfields for a change in a single variable. In this section results are presented for the whole test matrix and for both experiments and CFD.

Figure 9 shows the change in stagnation pressure coefficient between the inlet and exit traverse planes. For both CFD and experiments, the case with 1% fin seal clearance and an upstream cavity tangential velocity of 0.4U are chosen as datum points. Therefore what is shown is how the change in stagnation pressure alters as fin seal clearance and upstream cavity tangential velocity changes. It also shows how well the CFD is capturing the delta changes compared to the measurements.

At an upstream cavity tangential velocity of 0.4U, both the experimental and CFD results show a 1% of dynamic head increase in stagnation pressure coefficient per 1% change in fin seal clearance. At 0.25U, the calculated increase in stagnation pressure change is slightly higher than the experiments at 1.15% of dynamic head, compared to 1% from the experiments. This trend does not hold at the highest cavity tangential velocities, as the shape of the curves changes for difference clearances.

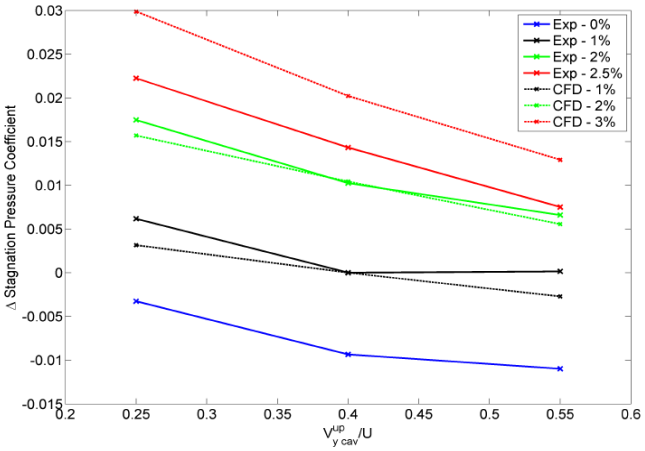

Figure 9: Change in stagnation pressure coefficient between the inlet and trailing edge traverse planes for CFD and experiments

Between 0.25U and 0.4U the experiments show that the stagnation pressure change reduced by approximately 0.6% of dynamic head for all fin seal clearances. A similar change is seen between 0.4U and 0.55U at the largest fin seal clearance. The CFD captures the trend of reduced stagnation pressure loss with increasing upstream cavity tangential velocity, however the magnitude of the change is less.

At low fin seal clearances, a distinct levelling off of the change in measured stagnation pressure coefficient can be seen at between 0.4U and 0.55U. The CFD do not show a linear change and the levelling off is significantly less pronounced than in the experiments.

The reason for the different shapes of the curves can be explained by the thicker boundary layer seen within the blade passage for the CFD calculations as mentioned above. As the turbulent CFD over predicts the growth of the endwall

boundary layers, the CFD calculations will see a larger amount of low momentum flow on the endwall leading to stronger secondary flows. Higher upstream cavity tangential velocities would be required (relative to the experiments) in order to offsets these secondary flows, hence why the CFD curves will only start to level off at higher upstream cavity tangential velocities.

Platform Geometry Effects

For the investigation into the impact of various platform geometry features, including 1% of pitch inter-platform gaps, 10% of pitch vane-pack gaps and misaligned hub platforms, the fin seal clearance was kept at 1% of span, however the upstream cavity tangential velocities were varied as before.

Inter-platform and vane-pack gaps

The hub geometry tested in the previous section included the 1% of pitch inter-platform gap, which is considered to be the baseline geometry for this study. For this investigation, the gaps were first covered over to give a smooth hub platform. Finally, one of the inter-platform gaps was increased in size to give a 10% of pitch vane-pack gap. As in a real engine, this gap does not appear in every passage, and only one gap was included in the cascade.

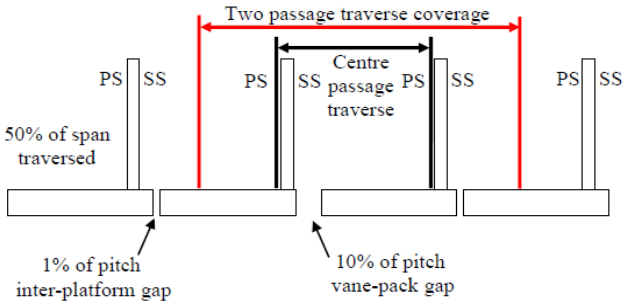

Figure 10: Location of vane-pack gap relative to the coverage of the traverse system as seen from the trailing edge of the cascade

For all previous cases, the change in stagnation pressure coefficients has been calculated from an average of the traverse plane spanning two blade passages. For the vane-pack gap the average is calculated for both the two-passage traverse, and for the centre passage as shown in Figure 10.

Figure 11 shows measured contours of stagnation pressure coefficient for a case with no hub platform gap, a 1% of pitch inter-platform gap in each passage and a 10% of pitch vane-pack gap in the centre passage. The differences between the smooth platform and 1% inter-platform gap cases are difficult to see, however there is a small area of low stagnation pressure coefficient centred just above the inter-platform gap that isn't present on the smooth endwall case.

Comparing the case with the 10% of pitch vane-pack gap against both the smooth endwall and datum cases reveals three main differences. The first, and most obvious, is the change to the hub corner loss cores on the left hand wake (at a fractional pitch of -0.25). The loss core is not as well formed as it is for the case with the datum platform and the intensity of the low stagnation pressure coefficient regions is reduced. The second change to note is the shape of the low stagnation pressure region along the hub endwall. In the centre passage of the traverse, this region of the flow has moved closer to the suction surface. The intensity of the low stagnation pressure region has also increased in the region directly above and just to the right of the gap. The third change to note is the change to the hub corner loss cores of the right hand wake (at a fractional pitch of 0.22). The size and intensity of the loss core decreases relative to the datum gap case. This indicates that the presence of the vane-pack gap affects not only the passage in which it is located, but also the passage adjacent to the pressure side of the passage with the large gap. It is not possible however, to determine the mechanism behind this change from the trailing edge traverses alone. CFD calculations were run and are presented later, however due to differences in the geometry setup the change to the flowfield in the adjacent passage is not seen. Further work would be required in order to investigate this flow feature fully.

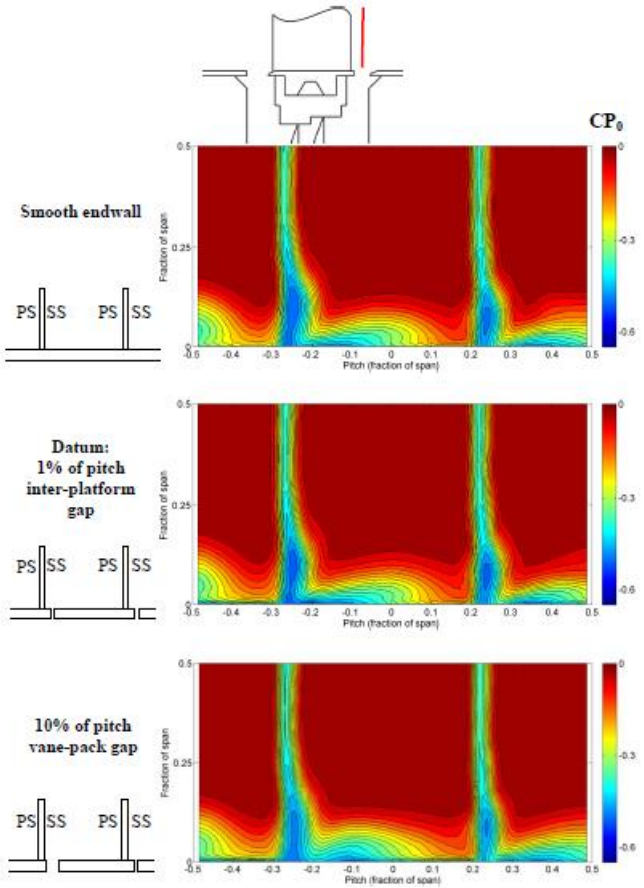

Figure 11: Measured stagnation pressure coefficient at the trailing edge for a smooth hub endwall, a datum 1% of pitch inter-platform gap and a 10% of pitch inter-platform gap (1% fin seal clearance and V_{ycav} = 0.4U)

Figure 12 shows the change in measured stagnation pressure coefficient between the inlet and exit traverse planes, relative to the datum geometry. The changes with fin seal clearance are shown for comparison to give an indication as to the magnitude of the change.

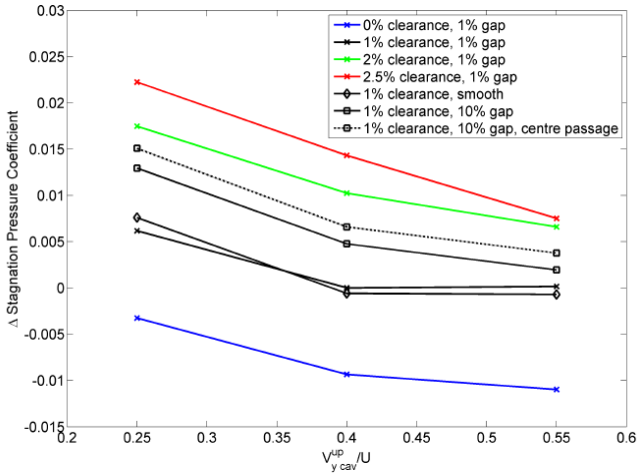

Figure 12: Change in measured mass-averaged stagnation pressure coefficient between showing the effect of the inter-platform and vane-pack gap versus a smooth endwall

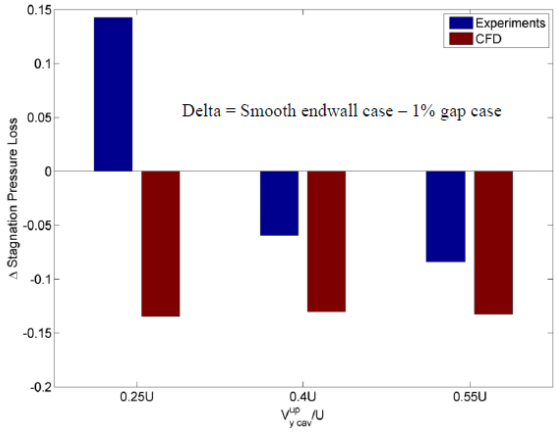

Figure 13: Comparison of the change in stagnation pressure coefficient between CFD and experiments for cases with and without inter-platform gaps.

Removing the inter-platform gap results in a reduction in the change of stagnation pressure of just over 0.1% of dynamic head for the two higher upstream cavity tangential velocities. At 0.25U this result is reversed with the smooth platform showing greater change in stagnation pressure coefficient. However, it should be stated that the levels of changes shown above are within the measurement accuracy of the traverse plane. The CFD results show a consistent reduction in stagnation pressure coefficient when the gap is removed, although the magnitude is slightly higher than that measured at the two higher upstream cavity tangential velocities. The comparison between CFD and experiments for the case with and without the inter-platform gaps can be seen in Figure 13.

The CFD results provide useful insight into the flow structure within the gaps and can help explain the above results. Figure 14 presents calculated streamlines which show the movement of the leakage flow within an inter-platform gap. The flow enters the gap from both the downstream cavity and from within the last thirds of axial chord and is driven upstream by the adverse pressure gradient within the blade row. The flow then re-enters the mainstream in the first third of axial chord where is undergoes turning and interacts with the gap region again towards the trailing edge. This flow structure helps explain the generation of the loss cores seen at the trailing edge. To further track the influence of the flow from the 1% inter-platform gap, and to also investigate the influence of the 10% vane-pack gap, slices are extracted from these two calculations as well as for the smooth endwall case, at four different axial locations.

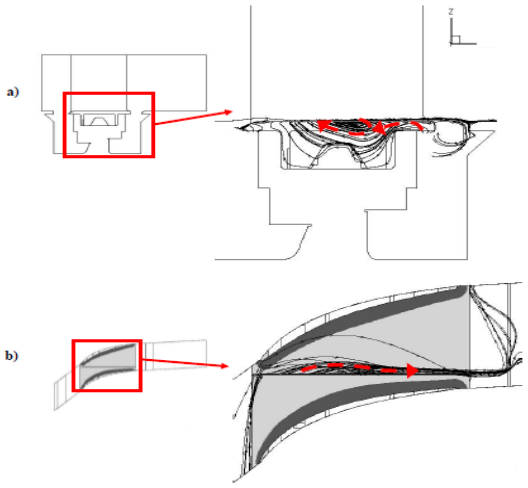

Figure 14: Calculated streamlines showing the progress of leakage flow through an inter-platform gap

Contours of stagnation pressure coefficient are shown for each of these slices and geometries in Figure 15. The first row shows the evolution of the hub flows for the smooth endwall case. With no discontinuities on the endwall the flowfield is smooth and there is a steady growth of the endwall boundary layer. With the presence of a 1% of pitch inter-platform gap, a region of low stagnation pressure fluid can be seen to accumulate on the pressure surface side of the gap. This is the fluid that exits the gap and re-enters the mainstream. The size of this region grows between the first and second slice planes as more fluid exits the gap. Progressing further down the passage the size of this low stagnation pressure region begins to reduce as fluid is being drawn down into the inter-platform gap. At the final slice plane the region has almost completely been removed and the flowfield is very similar to that of the smooth endwall case. This is the reason the two cases show similar results at the trailing edge traverse plane.

The 10% of pitch vane-pack gap has a larger effect due to the fact that more flow is able to move along the gap. Tracking the changes of the endwall flows in Figure 15 shows a large region of low stagnation pressure above and to the right of the gap. As with the 1% of pitch gap, this region grows in the first half of the passage but reduces in size towards the trailing edge. However as the volume of flow through the gap is much greater in this case, it is reinjected higher into the mainstream and hence it has a greater presence at the trailing edge. Flow near the trailing edge is drawn down into the gap at the trailing edge, which is located

right next to the suction side hub corner fillet, rather than feeding into the loss cores. This movement of the flow provides an explanation as to why the experiments showed reduced strength of the loss cores when a 10% of pitch gap was present.

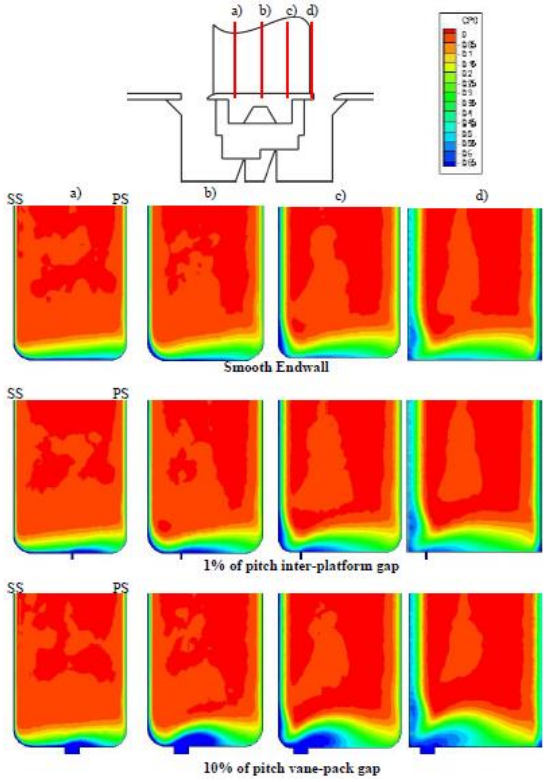

Figure 15: Calculated contours of stagnation pressure coefficient at various axial location within the passage for the three different gap cases.

Misaligned hub platforms

During assembly it is possible for hub platforms to become misaligned relative to one another. This misalignment is estimated to be up to 1% of span and results in a step between pressure surface and suction surface sides of the inter-platform gap. Two configurations were tested in the cascade and by CFD, although there are minor differences in the setup between the two. Ideally in order to maintain the blade passage area, one side of the passage should be raised by 0.5% of span, while the other reduced by the same amount. However this would involve changing all the hub platforms in the cascade for each configuration. As only the centre two can be easily changed, the steps were introduced by increasing the platform height of one of the two central platforms in turn, as shown in the cartoons. Traverse results at the trailing edge are shown in Figure 16. It should be noted that the PS High case actually shows both step configurations with the right passage showing SS High.

Comparing the contour plots of the pressure surface high case against the datum platform shows an increase in the size and spanwise extent of the loss core on the wake on the suction surface side of the centre passage. All across the hub wall there is an intense region of low stagnation pressure coefficient. This is due to the increased hub line, so the probe is reading below the level of the hub.

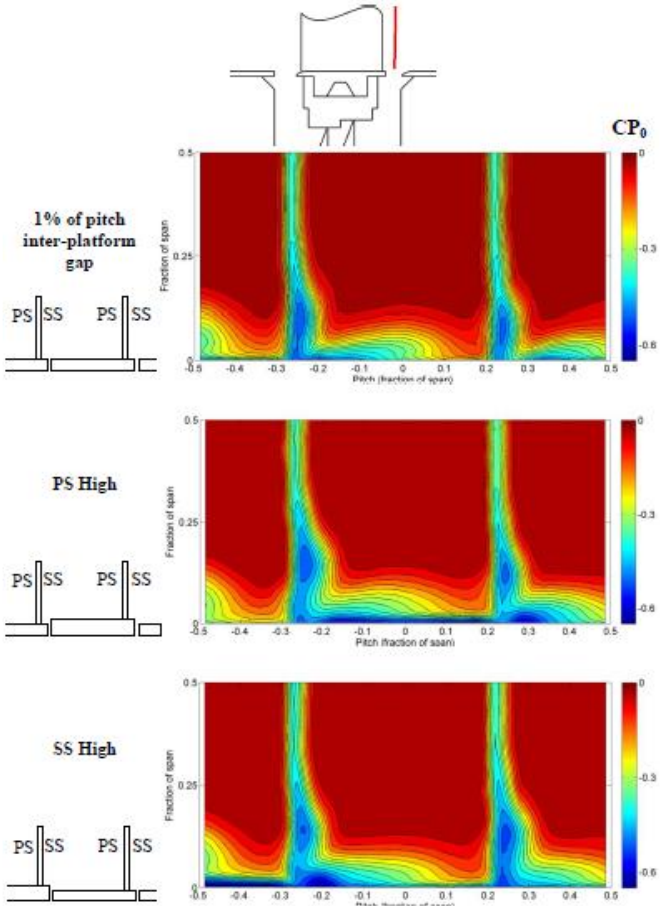

Figure 16: Contours of measured stagnation pressure coefficient for misaligned and aligned hub platforms

Figure 16 also shows the change between the suction side high and the datum cases. This shows that the loss core has slightly increased in size relative to the datum case and has also increased in spanwise location (although some of this increase is due to the hub platform being raised in this area). The changes seen for this configuration are not as pronounced as for the pressure side high configuration. The most obvious change is the intense region of low stagnation pressure coefficient accumulated up against the face of the step at a fractional pitch value of 0.2 of span. This lines up with the location of the step in the hub platform at the trailing edge. The same feature can be seen on the right hand passage of the pressure side high case which has the same orientation step as the suction side high case.

The overall change in measured stagnation pressure coefficient as a result of the presence of a step in the hub platform are shown in Figure 17. The results show that a step of either alignment increased the change in stagnation pressure coefficient relative to a smooth hub platform. The tests show that the PS High case has the larger deleterious effect of the two configurations, however this will be slightly skewed by region of low stagnation pressure present where the traverse covers the region just below the hub.

The CFD results also show both configurations increase the stagnation pressure change through the passage but the ranking of the misalignments is reversed relative to the tests.

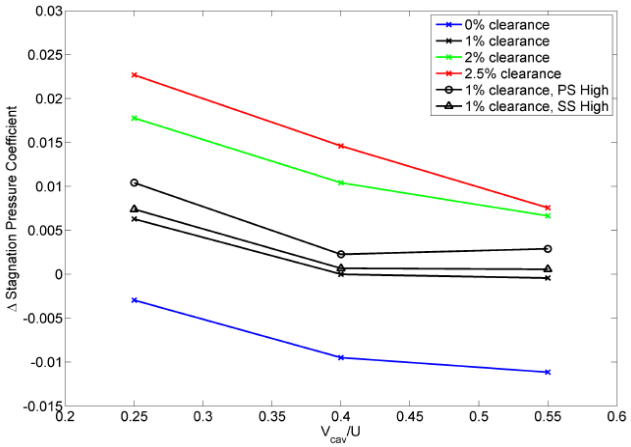

Figure 17: Overall change in stagnation pressure coefficient as a result of misaligned hub platforms

Conclusions

While the primary focus has been to investigate the impacts of real geometry features on the performance of a blade row, the investigation first highlighted the importance of boundary layer skew. The natural skewing of a boundary layer in a compressor helps to offset the secondary flows. Typical linear cascades would feature a collateral boundary layer and would therefore have larger secondary flow structures than would be seen in a compressor. For realistic endwall flow structures a novel method was developed to introduce a skewed boundary layer. The method involves injecting flow along the endwall at an angle to the mainstream flow. Careful selection of the flow rate and blowing angle allowed for control of the boundary layer displacement and tangential momentum thicknesses.

While the deleterious effects of increased shroud leakage are well known, the results presented in this paper show the combined effect of leakage and whirl pickup. For the majority of cases tested, a 1% increase in fin seal clearance results in a 1% increase in the change of stagnation pressure coefficient. Increasing the tangential velocity in the upstream shroud cavity has the effect of offsetting the secondary flows and as a result reduces the change in the stagnation pressure coefficient. Increasing from 0.25U to 0.4U results in a 0.6% of dynamic head reduction in the change of stagnation pressure coefficient. This is seen at all fin seal clearances. At higher upstream cavity tangential velocities, and at small fin seal clearances (≤1% of span) the reduction of the change in stagnation pressure coefficient starts to level off as the endwall flows are kept on the hub and their interaction with the suction surface is reduced. Increased fin seal clearances result in higher leakage flows but also lower upstream cavity tangential velocities, both of which are detrimental to blade row performance.

The tests and CFD calculations shown that steps and gaps on the endwalls have a deleterious effect on blade row performance. Within the gaps, flow is able to recirculate upstream where upon reinjection it causes a change to the local flowfield enhancing the secondary flow. Table 3 shows a ranked list of the impacts of the different real geometry features discussed within this paper.

Table 3: Impact of real-geometry features

Real Geometry Feature	ΔCP_0
1% of span fin seal clearance	1.02%
1% of span pressure surface high step	0.28%
1% of span suction surface high step	0.12%
10% of pitch vane-pack gap (assuming 1 every 8 passages)	0.08%
1% of pitch inter-platform gap	0.06%

This table shows that fin seal clearance and the resulting shroud leakage dominates the losses within a shrouded blade row. As at higher clearances, the whirl pickup will also be reduced, so maintaining as small as possible fin seal clearance must remain a priority. Misaligned endwalls cause the next largest increase of loss within a blade row and therefore minimising variations in manufacture and assembly must be emphasised. While the impact of gaps on the endwall is the smallest effect, keeping the gaps as small as possible, and reducing the number of vane-pack gaps, will help improve overall efficiency.

NOMENCLATURE

CP_0	Stagnation pressure coefficient $(p_0 - p_{0ref})/(p_{0ref} - p_{ref})$
U	Notional blade speed
V_x, V_y	Freestream axial, tangential velocity
v_x, v_y	Boundary layer axial, tangential velocity
δ^*	Displacement thickness, Eqn. 1.
θ_x	Axial momentum thickness, Eqn. 2.
θ_y	Tangential momentum thickness, Eqn. 3.

ACKNOWLEDGEMENTS

The authors thank both Rolls-Royce plc and EPSRC for funding this work and are grateful for the permission of Rolls-Royce to publish.

REFERENCES

Demargne, AAJ. Longley, JP. 2000. *The Aerodynamic Interaction of Stator Shroud Leakage and Mainstream Flows in Compressors*. ASME Paper 2000-GT-570.

Denton, JD. 1993. *The 1993 IGTI Scholar Lecture: Loss Mechanisms in Turbomachines*. ASME Journal of Turbomachinery, Volume 115 Nº 4, pp 621-656.

Gbadebo, SA. Cumpsty, NA. Hynes, TP. 2004. *Three-dimensional separations in axial compressors.* Proceedings of the ASME Turbo Expo 2004, GT2004-53617.

Grewe, Robert P. Miller, Robert J. Hodson, Howard P; *The effect of endwall manufacturing variations on turbine performance*. ASME Paper GT2014-25326

Heidegger, NJ. Hall, EJ. Delaney, RA. 1996. *Parameterized study of high-speed compressor seal cavity flow*. AIAA Paper 96-2807.

IATA, 2017. Economic Performance of the Airline Industry. http://www.iata.org/publications/economics/Reports/Industry-Econ-Performance/IATA-Economic-Performance-of-the-Industry-end-year-2017-report.pdf [5th December 2017]

Leishman, BA. Cumpsty, NA. Denton JD. 2004. *Effects of bleed rate and endwall location on the aerodynamic behaviour of a circular hole bleed off-take.* ASME Paper GT2004-54197.

LeJambre, CR. Zacharais, RM. Biederman, BP. Gleixner, AJ. Yetka, CJ. 1998. *Development and Application of a Multistage Navier-Stokes Flow Solver: Part II – Application to a High-Pressure Compressor Design*. ASME Journal of Turbomachinery, Vol. 120, pp. 215-223.

Mager, A. 1952. *Generalisation of boundary-layer momentum-integral equations to three-dimensional flows including those of rotating systems.* National Advisory Committee for Aeronautics, Report 1067.

Moore, RW. Richardson, DL. 1957. *Skewed Boundary-Layer Flow Near the End Walls of a Compressor Cascade*. Transactions of the ASME, Volume 79, pp 1789-1800.

Öztürk, HK. Turner, AB. Childs, PRN. Bayley, FJ. 2000. *Stator well flows in axial compressors.* International Journal of Heat and Fluid Flow, Volume 21, pp 710-716.

Reid, K. Denton, J. Pullan, G. Curtis, E. Longley, J. 2005. *The Interaction of Turbine Inter-Platform Leakage Flow with the Mainstream Flow*. ASME Paper GT2005-68151.

Sieverding, CH. 1984. *Recent Progress in the Understanding of Basic Aspects of Secondary Flows in Turbine Blade Passages*. Transactions of the ASME, Journal of Engineering for Power, 84-GT-78.

Wellborn, SR. Okiishi, TH. 1998. *The Influence of Shrouded stator Cavity Flows on Multistage Compressor Performance*. ASME Paper 98-GT-12.